Experimental Analysis of a Shake Table Test of Timber-Framed Structures with Stone and Earth Infill

F. Vieux-Champagne,[a),b),c)] Y. Sieffert,[b),c)] S. Grange,[b),c)] C. Belinga Nko'ol,[a)] E. Bertrand,[d)] J. C. Duccini,[e)] C. Faye,[e)] and L. Daudeville[b),c)]

The seismic performance of timber-framed structures filled with stones and earth mortar has been analyzed by introducing the structural subscales (cell, wall, house) at which monotonic and cyclic loadings were considered. This article aims to present the dynamic behavior of a house as determined through shaking table tests. Based on this experimental multiscale analysis, this paper confirms that timbered masonry structures offer effective seismic resistance; moreover, such a comprehensive analysis helps enhance understanding of the seismic-resistant behavior of timber-framed structures with infill. This paper also aids ongoing development of a numerical tool intended to predict the seismic-resistant behavior of this type of structure. [DOI: 10.1193/010516EQS002M]

INTRODUCTION

According to Gurpinar et al. (1981), the existence of timber-framed structures with infill dates back several millennia, having originated in the Neo-Hittite states (northern Syria and southern Turkey), where timber-framed structures filled with adobe were already widespread. In Italy, an archaeological excavation campaign in Herculaneum revealed a building during Roman times featuring two levels of wood-framed structure with infill. This type of structure was listed under the name of *Craticii* or *Opus Craticium* by Vitruvius (Langenbach 2007). Moreover, such buildings are found throughout the world (Vieux-Champagne et al. 2014) and are still being built in most countries.

Timbered masonry structures are popular worldwide mainly for their reduced construction cost, thanks to the use of local resources and know-how, as well as for their aesthetics and/or ability to achieve greater resistance to seismic forces (see Dutu et al. 2012). Traditional timbered-framed structures with infill have indeed exhibited remarkable behavior during recent major earthquakes (Turkey in 1999, Greece in 2003, Kashmir in 2005, Haiti in 2010, or China in 2013), often sustaining very little damage. In contrast, the seismic-resistant behavior of new construction made of masonry blocks or concrete has generally been subpar or even disastrous (Haiti in 2010). Haiti's problems stemmed from the lack of a building code

[a)] CRAterre, AE&CC Research Unit, National School of Architecture of Grenoble, France
[b)] Univ. Grenoble Alpes, 3SR, F-38000 Grenoble, France
[c)] CNRS, 3SR, F-38000 Grenoble, France
[d)] CEREMA, Laboratoire de Nice, F-06300 Nice, France
[e)] FCBA, French Technological Institute for Forestry, Cellulose, Timber Construction and Furniture

and standards for designing structures, which was due to the fact that seismic forces tend not to be considered in the design of most engineered buildings, as well as to the presence of poor quality construction and/or materials (see Paultre et al. 2013 and Dogangun et al. 2006). Ensuring a structural implementation that meets building codes carries with it a relatively high cost, thus making modern construction techniques inaccessible to the majority of localities (Tobriner 2000, Makarios and Demosthenous 2006, Langenbach 2008, Audefroy 2011, and Qu et al. 2014).

These findings raise an issue concerning the minimal importance assigned to local architecture by the scientific community, as well as by those responsible for reconstruction efforts. A number of research projects have recently been conducted to enhance knowledge of the seismic-resistant behavior with respect to traditional wood-framed structures with infill. As regards experimental works, the following authors, whose scale of investigation has ranged from the connection to the shear wall, can be cited (see Figure 1):

- Connection: Ali et al. (2012) ("Dhajji-Dewari" construction);
- Elementary cell: Ferreira et al. (2012) ("Pombalino" construction);
- Reduced scale of a shear wall: Cruz et al. (2001) ("Pombalino" construction) and Vasconcelos et al. (2013) ("Pombalino" construction);
- Shear wall: Meireles et al. (2012) ("Pombalino" construction), Poletti and Vasconcelos (2014) ("Pombalino" construction), Ali et al. (2012), Ceccotti et al. (2004) ("Maso" construction), Aktas et al. (2013) ("Himis" construction);
- Building: none, to the best of the authors' knowledge.

All these shear tests are based on a quasi-static loading and corroborate the good seismic resistance of such structures, even though structurally speaking they are quite distinct.

This paper will present the experimental study of a timbered masonry structure in Haiti, called "Kay peyi," in an attempt to analyze its behavior under seismic loads. The aim here is to offer a scientific assessment of the structure's implementation. This work program is based on specific buildings, as shown in Figure 2, built as part of different Haitian reconstruction projects (i.e., Misereor, SC/CF projects in collaboration with the CRAterre laboratory and local partners, such as the Haitian NGO "GADRU").

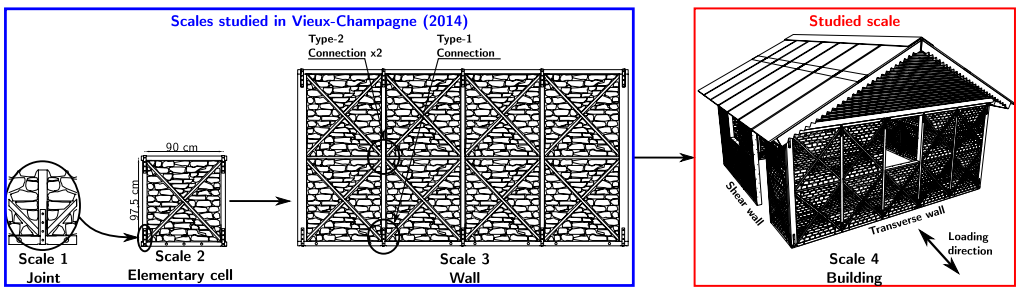

Figure 1. The four scales of this experimental study (house model sketched by C. Belinga Nko'o).

(a) Traditional (b) Built for a reconstruction project

Figure 2. Rural Haitian houses.

This dynamic structural behavior will be studied at scale 4 (building) in order to complete the first part of the quasi-static experimental campaign, which encompasses the connection (scale 1) and the elementary cell (scale 2) and extends to the shear wall (scale 3, Vieux-Champagne et al. 2014). This multiscale approach is illustrated in Figure 1.

Such an approach provides an understanding of the behavior of the various wall components. At the first scale, type-1 connections will be studied to determine the local influence of the nail number under two loading directions. The elementary cell scale then serves to analyze the influence of the type and presence of infill. Scale 3 (wall) will be examined as a means of emphasizing the structure's overall behavior. Lastly, scale 4 (house) provides a complete understanding of the structure, as regards the dynamic behavior of the transverse walls, the in-plane wall, the roof, and the connections at the wall–roof interface.

For purposes of this study:

- A representative ground motion of Haiti's 2010 earthquake has been designed (100% deterministic), based on both the local seismic context and typical Port-au-Prince soil;
- A seismic signal calibrated on acceleration spectra, representative of Guadeloupe's high seismic hazard zone (Bertil et al. 2010), has been introduced.

These signals yield an analysis of the structure under the actual Haitian ground motion, a ground motion that complies with current regulations, and a high-frequency range capable of optimizing shake table capacity.

This article is divided into three parts: The first section will present the test building and materials used in its construction. Next, the second section will describe the shake table test program (experimental set-up, instrumentation, and the simulated ground motion), while the last section will report and discuss the results of this campaign.

TEST BUILDING AND MATERIALS

Filled wood structures are built in many countries (including France, Germany, Italy, Pakistan, India and Haiti) (see Langenbach 2006, Makarios and Demosthenous 2006, and Dogangun et al. 2006), in recognition of the use in most cases of natural materials available on-site. This solution therefore is environmentally friendly (a key concern in developed countries), while offering simpler building conditions and a lower cost (major considerations in emerging countries).

Three main types of such structures are prevalent in Haitian rural reconstruction projects: (1) bracing by means of San Andrew's crosses (X-cross), filled with natural stones and bonded by an earth mortar (see Figure 2); (2) bracing with just one diagonal and filled with adobe (handmade earth brick); and (3) bracing by wattle and daub (W & D) panels (with a frame made of pieces of wood or bamboo) and filled by earth mortar. The X-cross wall filled with stones was selected for this study by virtue of being easiest to build and thus the most widespread. The X-crosses simplify filling of the structure and enhance safety in the case of falling stones thanks to smaller-sized infill components. Large pieces of wood however are more difficult to procure by the local population.

The house has a footprint of $4.65 \times 4.65\ m^2$; it is 3.20 m high (at the ridge) and symmetrical about the N–S axis (i.e., the loading direction, see Figure 6). The shear walls have six vertical posts, with a window and door respectively between posts 2–3 and 4–5 in the N–S direction. The transverse walls are identical, with six vertical posts as well and one window located between posts 3 and 4. The specimen was anchored into steel beams by means of 40 bolts (two between each pair of vertical posts, which were themselves bolted onto the table; see Figures 5b and 5c).

The earth is composed of a 4/1 ratio of a 0–25 mm sifted clayey earth, a 1/2 ratio of water (depending on the water content of sand) and a 1/1 ratio (very coarse measurement) of sisal fibers (easily available in Haiti). To prevent the mortar from cracking, water content must be limited in the earth and moreover sisal fibers need to be added.

These fibers serve to limit the onset of cracking and its propagation in the mortar. Plain shank nails (also called "common nails" or "wooden nails") are placed inside wood triangles in order to improve the bond between both parts.

The bracings are composed of Saint Andrew's crosses with one continuous diagonal and another diagonal divided into two parts (Figure 1); they are connected to the vertical post using two 70 mm long wooden nails (Figure 3b). These techniques facilitate construction and avoid weakening the wood, as opposed to an edge half-lap joint located at the center of each diagonal.

Various connections have been used to build the structure described above (see Figure 3), though not all of them exert the same influence on the seismic resistance of the structure. The type 1 is a steel–wood nailed joint (Figure 3a), which consists of a punched steel strip surrounding the wood parts (in a T-shape) and fastened by a few nails that determine the behavior of the connection. The type 2 is the joint between the middle of the post, the bracings, and the nogging (i.e., the middle horizontal stud) (Figure 3b). The connection between the roof and the walls is made by ligature wire, as

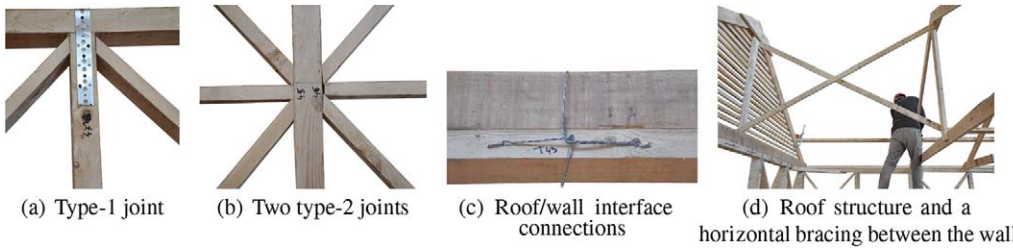

Figure 3. Nail connections of the timber structure.

depicted in Figure 3c. The remaining connections (horizontal diaphragm and roof structure, Figure 3d) are nailed joints.

The timber strength class is C18, with a density $\rho_{\text{mean,C18}} = 390\,\text{kg/m}^3$ according to European Standard EN 338 (see EN 338 2003). The strip is an FP30/1.5/50 from Simpson Strong-Tie®, 30 mm wide and 1.5 mm thick. 3×70 mm plain shank nails were used (see EN 10230-1 2000) to fasten the strip.

The roof was made with 28 2.5×0.9 m^2 metal sheets 0.5 mm wide (6 kg) fastened to the timber structure by means of nails.

SHAKE TABLE TEST PROGRAM

A dynamic test has been conducted on an entire timber-framed house with walls filled by both earth and stones and whose design has been adapted from the Haitian building culture specifically for purposes of this study (see the "Acknowledgements" section). This test was intended to analyze the behavior of such a structure under seismic loading.

EXPERIMENTAL SETUP

Shake Table

These dynamic tests were performed at the uniaxial earthquake simulation facility in the Mechanical Laboratory of the French Institute FCBA. The shake table is composed of a 6×6 m^2 aluminum platform moved by a 250 kN servo-hydraulic actuator (Figure 4).

Shaking Table–Structure Interface

Since the house contains infill panels, it had to be built directly on the table in order to prevent cracks in the earth. A steel frame was designed to anchor the structure onto the table, as depicted in Figure 5. The mudsill was locked into the steel frame by means of a wooden wedge (Figure 5c) and then bolted to it. This study is focused on seismic response of the timber frame structure with infill and doesn't take into account the foundation and its connection to the wooden structure. It is assumed that the structure is perfectly connected to the foundation that is considered as rigid body. Obviously, the failure location depends on the nature of the structure and of the soil–structure interactions, but in terms of design, the objective is to make it happen into the steel fasteners of the mudsill to post connections.

Dimensions	6×6	m2
Weight	6	tons
Max. dis.	$\pm$ 0.125	m
Max. vel.	0.75	m/s
Max. acc.	4	g
Frequency range	0 - 30	Hz

Figure 4. Shake table characteristics.

(a) Timber structure anchored into the steel frame

(b) Mudsill placed in the steel frame

(c) Mudsill locked by a wooden wedge

Figure 5. Anchorage of the structure on the shake table.

Seismic Test Sequence (See Table 1)

As indicated above, this test sought to analyze the behavior of this kind of structure under seismic loading. For this purpose, the seismic loading had to be representative of Haiti's 12 January 2010 earthquake. Unfortunately, this signal could not be recorded but was instead designed according to the empirical Green's function method. This simulated signal is the so-called Haiti (HTI) 100% in this paper (see Section 3.3.1). Next, in order to analyze the nonlinear behavior of the structure, the house was subjected to the 200% and 300% signal as well as to a Guadeloupe (GUA) far-field ground motion (Section 3.3.2). Between the HTI and GUA signals, the structures were repaired. The reparation process consisted of hammering back the extracted nails and tightening the loosened ligature wires. To assess the change in fundamental frequency, the structure was subjected to low-level white noise [0.03 g and 0.5 mm root mean square (RMS)] between each seismic loading.

INSTRUMENTATION

The measurement devices used were placed according to the layout shown in Figure 6. The accelerometers allowed analyzing the natural frequency evolution, while the draw wire

Table 1. Seismic test sequence

Seismic test level	Ground motion	Seismic hazard level	Amplitude scaling factor	Scaled PGA (g)
1	HTI	—	1	0.27
2				0.54
3				0.77
Reparation operation				
4	GUA	10%/50Y	1	0.32
Reparation operation				
5	GUA	—	3.9	1.26

displacement sensor (DWDS) and linear variable differential transformer (LVDT) measurements were compared to results of the digital image correlation (DIC) produced through high-speed camera pictures, with a subsequent comparison to numerical modeling results. To the best of the authors' knowledge, this constitutes the first time a DIC has been used to analyze this kind of structure at this scale. As such, let us now focus on the set-up introduced to perform the DIC.

The Phantom v641 high-speed camera (with a 28 mm lens, 4 megapixels) was used to capture the eastern shear wall, at a speed of 150 frames per second (fps), in order to obtain the absolute displacement field of the panel by DIC. The acquisition rate was set to be higher than the frequencies contained in the seismic signal (<30 Hz, i.e., for a minimum of 30 fps). The speckled pattern was generated by projecting black, gray, and white paints. The average speckle dot diameter was approximately 1 cm. The lighting (4,000 W, 4 K alpha version)

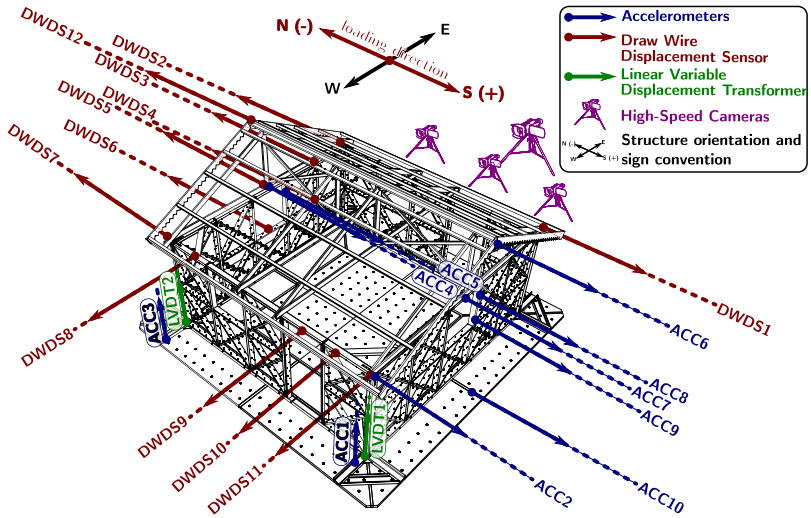

Figure 6. Measurement device position and sign convention.

was placed 5 m from the wall. This powerful projector was necessary to produce a uniform and intense lighting. Once the videos were recorded, kinematic field measurements could be performed by means of a DIC technique with the Tracker software developed by Combe and Richefeu (2013). Measurement accuracy was about 0.1 pixel or 0.22 mm across the building.

SIMULATED GROUND MOTIONS

For purposes of this research, a strong ground motion had to be simulated since no seismological recording of the 12 January 2010 earthquake is available in Port-au-Prince. Two signals were simulated, the first corresponding to a Mw 6.8 earthquake occurring 34 km west of Port-au-Prince, and the second one fitting an empirical response spectrum characteristic of seismic activity in the French West Indies.

Haiti Ground Motion

Context

Port-au-Prince is located at the southern edge of the Cul de Sac Valley, which is a large rift valley extending east-to-west from the Haitian coast to the Dominican Republic. Most of the valley is underlain by young sediments (Lambert et al. 1987), while most of the city of Port-au-Prince is underlain by Mio-Pliocene deposits including marl, sandstone, siltstone, and shale in alluvial fans and low foothills (Lambert et al. 1987). The Mio-Pliocene deposits are expected to be relatively stiff compared to younger, less consolidated Quaternary deposits (Hough et al. 2010); however, they are also expected to be characterized by lower impedance than the adjacent hills to the south, which are composed of more highly consolidated limestone, conglomerate, and volcaniclastic rock (Lambert et al. 1987). Some degree of sediment-induced amplification is therefore expected throughout Port-au-Prince.

Methodology

Seismic ground motion can be predicted by numerically modeling wave propagation. Most methods include the source complexity and travel path from the source to the surface. These deterministic methods, however, are insufficient to accurately predict seismic motion above a few hertz. The resulting ground motion also depends to a great extent on velocity model accuracy; hence, most models do not consider amplifications due to Quaternary deposits.

To predict broadband ground motion, an empirical approach based on the site-specific empirical Green's function (EGF) technique (e.g., Hartzell 1978) was adopted. This simulation leads to synthetic ground motion that can be useful for the engineering community regarding the seismic design and assessment of civil structures. The seismic motion, capable of being generated in Port-au-Prince, was simulated in considering a scenario using a location near the 2010 earthquake site. This motion has been simulated for a site exhibiting strong local effects in the center of Port-au-Prince nearest the targeted epicenter (HVPR, USGS-BME) (Altidor et al. 2010, Hough et al. 2010). The simulated earthquake has a moment magnitude equal to 6.8, with a location 34 km from the HVPR station and a focal depth of 12 km.

The method employed is based on the hypothesis of similarity between earthquakes of differing magnitudes, in considering that both weak and strong earthquakes are similar processes that differ by a scaling factor. The underlying principle is to simulate the recordings of

a hypothetical future earthquake using the actual recordings of a smaller one that contains rich information on path and site effects. The stochastic approach proposed by Kohrs-Sansorny et al. (2005) was implemented. This method is based on a two-step summation scheme. The SIMULSTOC code offers the advantage of requiring only a few input parameters while rapidly generating a large number of possible accelerograms. This method is also based on the works of Boore (1983), Wennerberg (1990), and Ordaz et al. (1995). In practice, 500 equivalent source time functions (ESTFs) were generated representing the time histories of the energy release over the fault at frequencies less than the corner frequency of the small event set as the EGF. A random, two-step process proposed by Ordaz et al. (1995), using two probability density functions, was adopted to generate these ESTFs, whose differences can indirectly account for the different types of ruptures and produce a large variability in ground motions (Beauval et al. 2009). Next, each ESTF was convolved with the EGF at the station corresponding to each component. The higher frequency part of the spectrum (>fc) was then directly modeled by the small event's spectrum. This method yields synthetic time histories that, on average, are in agreement with the ω^{-2} model (Aki 1967 and Brune 1970) and moreover respect a nonconstant stress-drop condition (Beeler et al. 2003 and Kanamori and Rivera 2004). All method details can be found in Kohrs-Sansorny et al. (2005). Among the requisite input parameters, the ratio between the static-stress drop of the target event C is the only one without an associated constraint. For a practical application in the present simulation, considering a C value of 1 is proposed.

The selected aftershock (taken as an empirical Green's function) occurred on 3 May 2010 (7:21 pm). Its moment magnitude was measured to be 4.4, and the epicenter was located close to Logne (18.538 N, 72.643 W). Since the north–south component of the EGF was strongest at the HVPR station, it was used in the Mw 6.8 ground motion simulation. From the 500 simulations, the one with the largest loading between 0.1 and 0.5 seconds of period length was selected. For low-rise structures, this simulation involves taking the worst-case scenario possible among our set of synthetics. The result, in terms of elastic response spectrum, is shown in Figure 7b; Figure 7a displays the corresponding time history in acceleration.

Guadeloupe Ground Motion

Another seismic signal was introduced in order to subject the structure to:

- A signal calibrated on an acceleration spectrum representative of high seismic hazard zones in the Antilles.
- A different frequency range.
- Optimized shake table capacities.

The generation of this modified natural accelerogram has been adapted from the Miyagi earthquake (Japan 2003), as measured at the K-Net station and calibrated on an earthquake spectrum by the relationship developed by Youngs et al. (1997; Guadeloupe scenario, far-field subduction ground motion), so as to improve spectrum representativeness. This finding is correlated with a scenario of "strong hazard," soil B from Eurocode 8 (EN 1998-1 2005), and a probabilistic computational basis with a 475 year return period. This corresponding seismic hazard level has a 10% probability of exceedance in 50 years (10%/50Y), which satisfies the probability associated with the non-collapse requirement in Eurocode 8.

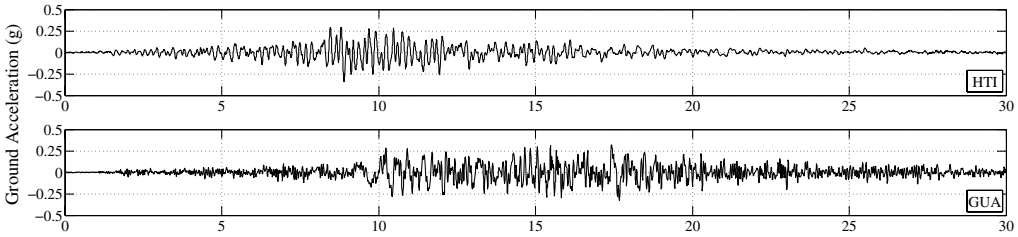

(a) Time-history of the ground motions

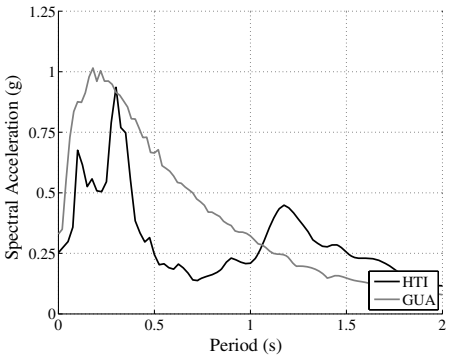

(b) Absolute acceleration response spectra for 5% damping of earthquake ground motions used in seismic tests

Figure 7. Time and frequency content of the Haiti (HTI) and Guadeloupe (GUA) ground motions.

The time and frequency content of the ground motion, as obtained by the method described above for the Guadeloupe far-field scenario (PGA = 0.33g), is indicated in Figure 7.

RESULTS AND DISCUSSION

Our results will be presented in three sections, namely: "free vibration tests" to evaluate the modal properties of the structure; "global building response"; and "observed damage," as is customary in articles focusing on the analysis of shake table tests at the structural scale (see Filiatrault et al. 2002, Filiatrault et al. 2009, Vande Lindt et al. 2010, vande Lindt et al. 2014, or Bahmani et al. 2014).

FREE VIBRATION TESTS

Before the seismic tests, a modal analysis was conducted by measuring three axis acceleration responses at each wood member intersection of the structure while subjected to a white noise excitation. This process yielded the first three modal shapes (Figure 8), natural frequencies, and damping ratios (Table 2). The first two modes are similar and represent the transverse wall modes (Figures 8a and 8b). The small frequency difference can be attributed to the various positions of openings in the shear wall, as well as the intrinsic

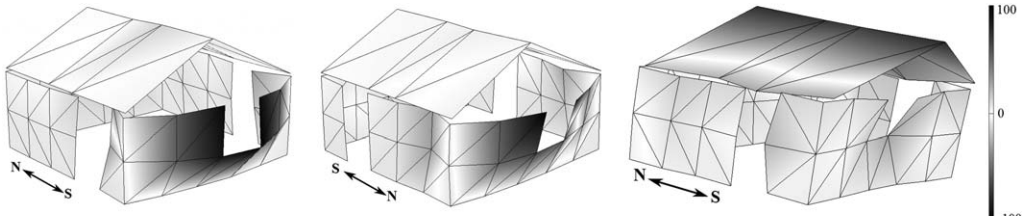

(a) First modal shape of the first transverse wall (b) First modal shape of the second transverse wall (c) Second modal shape of the shear wall

Figure 8. Fundamental modal shapes of the structures, as obtained through the modal analysis performed before the seismic tests.

differences in the workmanship of the two walls (weight, geometric dimensions, etc.). The second primary mode is the shear wall vibration (Figure 8c).

At the initial state and after seismic tests, a modal structure was excited by a low-level white noise base acceleration input with a uniform spectrum (0.5–25 Hz frequency band), a RMS amplitude of 0.03 g and 0.5 mm for the purpose of evaluating both the frequency drop in the structure and the destructiveness of previous input signals. An analysis of the structural modification resulting from successive seismic tests was performed by computing:

- the frequency response function (FRF, Figure 9) between the output acceleration at node 7 (ACC7) and the input table acceleration (ACC10) obtained during each low-level white noise input test (Figure 6). As a reminder, the FRF is a representation in the frequency domain of the ratio between an output and input acceleration signals;
- the deterioration of the normalized equivalent lateral stiffness (NELS) in the N–S direction after each seismic test (Figure 10a), in assuming a single-degree-of-freedom response of the test building. Since the initial fundamental period T_0 is known, as is the fundamental period T_i measured after each seismic test, the NELS k_i as a percentage of initial lateral stiffness k_0 can be calculated after each seismic test as

$$\frac{k_i}{k_0} = \left(\frac{T_0}{T_i}\right)^2. \tag{1}$$

Table 2. Natural frequencies and the equivalent viscous damping ratio

Pole	Element	Frequency (Hz)	Damping ratio (%)
1a	Transverse wall	5.2	5.2
1b	Transverse wall	5.9	5.7
2	Shear wall	10.9	5.3

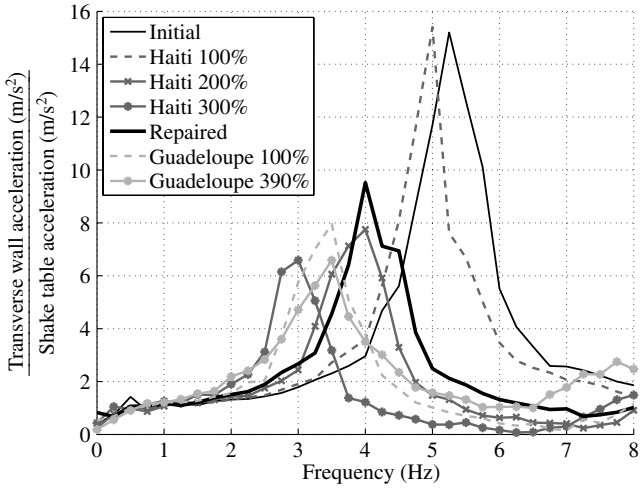

Figure 9. Frequency response function of the transverse wall acceleration to the shake table acceleration.

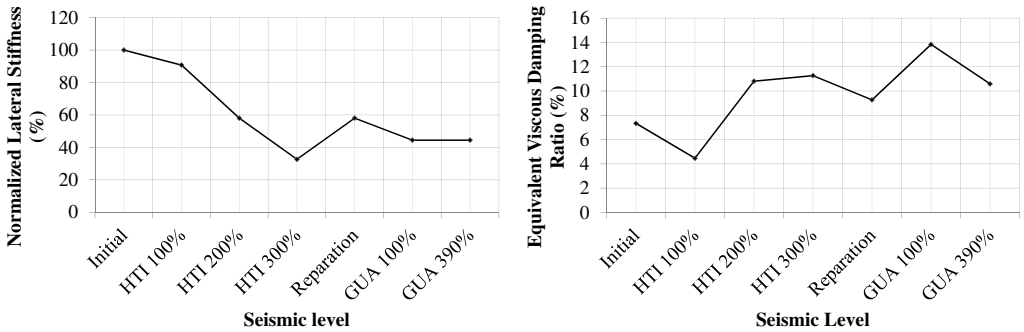

(a) Variations of normalized lateral stiffness

(b) Variations of first modal damping ratios

Figure 10. Variation of seismic indicators.

The NELS remains proportional to the natural frequency of the structure:

- the variations in the first modal equivalent viscous damping ratio (EVDR) measured in the N–S direction of the test building after each seismic test conducted (Figure 10(b)). The EVDR of the test building was determined using the half-power bandwidth method (see, for example, Clough and Penzien 1993) applied to the FRF peaks.

By means of these graphs, it is now possible to analyze the evolution in structural damage. In other words:

- HTI 100%: After the "HTI 100%" seismic test, acceleration remained constant while the natural frequency (and hence the normalized stiffness) decreased by 4.8% (Figures 9 and 10a). This outcome is due to a slight rearrangement of the wood–earth interface, involving the removal of some friction interfaces between the two materials, which would also explain the decrease in NELS shown in Figure 10a.
- HTI 200%: After this signal, a significant reduction in both the natural frequency (5 Hz to 4 Hz, i.e., equivalent to a decrease in NELS of approximately 30%) and amplitude (15.4 to 7.8) are recorded, while the EVDR rises by around 6 points. These results stem from damage to the steel connections (buckling of steel strips, nails pulled out, loosening of the ligature wires, and degradation of the wood–earth interface, Figure 20).
- HTI 300%: In this case, the natural frequency, acceleration amplitude, and NELS all followed the same trend as in HTI 200%, whereas the EVDR increased very slightly. This finding can be explained by the fact that the same deterioration processes occurred during "HTI 200%" and "HTI 300%" (Figures 20b and 20e); therefore, the EVDR and energy dissipation were not much higher than during the "HTI 200%" test.
- Repairing: After this process, the structure returned to the level of natural frequency obtained during the HTI 200% test; in contrast and as logically expected, the acceleration amplitude increased and the EVDR dropped.
- GUA 100%: After this test, it is worthwhile to note that despite the relative harmfulness of the seismic signal (in comparison with the two previous ones and the next one), the energy dissipation shown in Figure 10b reached a maximum value due to damage to the repaired connections, which is correlated to a decrease in both the NELS and acceleration amplitude.
- GUA 390%: After this seismic level, a portion of the filling collapsed (Figure 20h), which significantly reduced the weight of the transverse walls. Despite the increase in overall structural damage, the NELS therefore remained constant while the acceleration amplitude and EVDR decreased.

GLOBAL BUILDING RESPONSE

This section aims to detail the analyses conducted relative to the global deformation and global hysteretic response.

Global Deformation

In order to obtain the absolute displacement in the structure, DWDS, LVDT sensors, and a high-speed camera were all employed. As explained above, this effort represents the first time that a high-speed camera has been used at this structural scale. It was therefore necessary to validate the results obtained by DIC; Figure 11 depicts the points tracked through the DIC. Figures 12 and 13 show the comparison of the displacement obtained on the shaking table by LVDT, DWDS, and by DIC for the various tests performed. The correlation between results from both measurement methods is quite good, thus validating the use of DIC.

Figure 11. Points whose displacement is analyzed by the DIC.

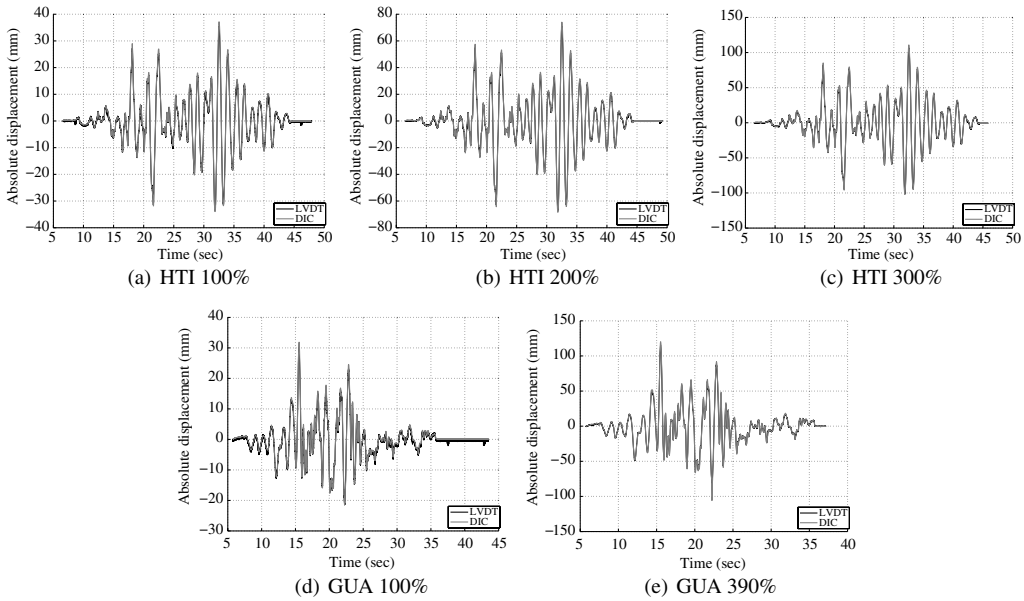

(a) HTI 100% (b) HTI 200% (c) HTI 300%

(d) GUA 100% (e) GUA 390%

Figure 12. Comparison of the absolute shake table displacements obtained by DIC and shake table LVDT (not represented in Figure 3.2).

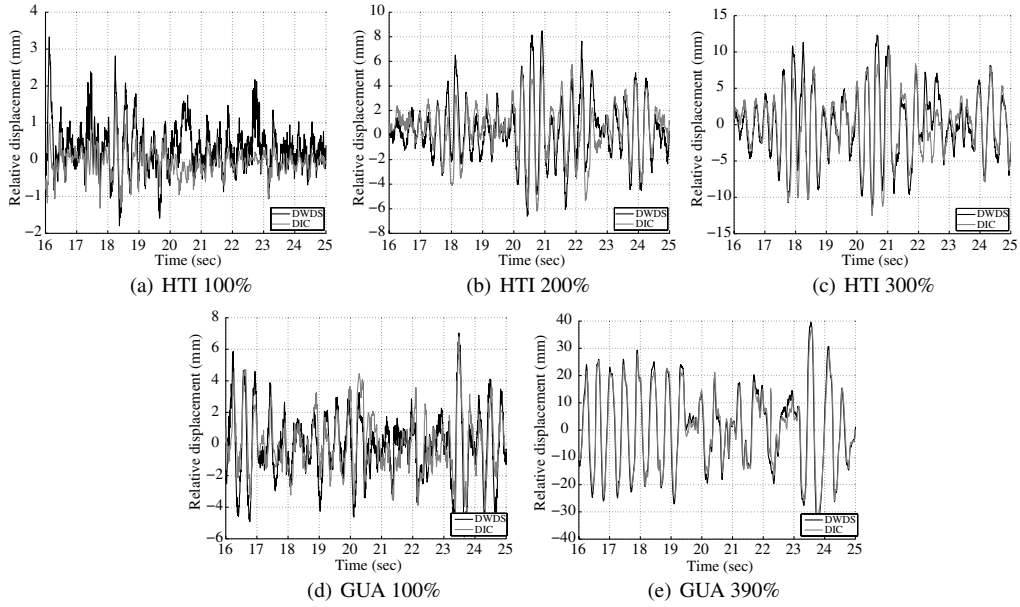

Figure 13. Comparison of the top relative wall displacements obtained by DIC and DWDS1.

Figure 15 indicates the maximum global deformation obtained during each seismic test. This depiction was obtained by adopting the following assumptions:

- The deformation shape of the structure is symmetrical about both the N–S and E–W axes (as illustrated in Figure 14).
- The deformation shape of the transverse beams of the transverse walls can be interpolated from the measures of the six DWDS.

Figure 15 highlights various phenomena, namely:

- Shear walls reach their maximum displacement almost always at the same time as the transverse walls. The deformation of both are indeed correlated.
- Structural damage affects the time when shear walls reach their maximum deformations as well as the underlying nonlinear evolution in these deformations. After each signal, the natural period of the building is in fact modified due to the damage sustained, thereby varying the structural response of the subsequent signal. For instance, during the HTI 100% signal, shear walls reached their maximum displacement 3.33 mm at 18.12 sec, while for HTI 200% this displacement equaled 8.49 mm (i.e., a factor of 2.55) at 20.91 sec. This finding reveals a distinct response of the building relative to the damage sustained; the present example is also true for other signals and transverse walls.
- The transverse wall deformation is much greater than that of the shear wall. This outcome can easily be explained by the absence of a stiff horizontal bracing structure to prevent this strong deformation and moreover by the fact that the connections

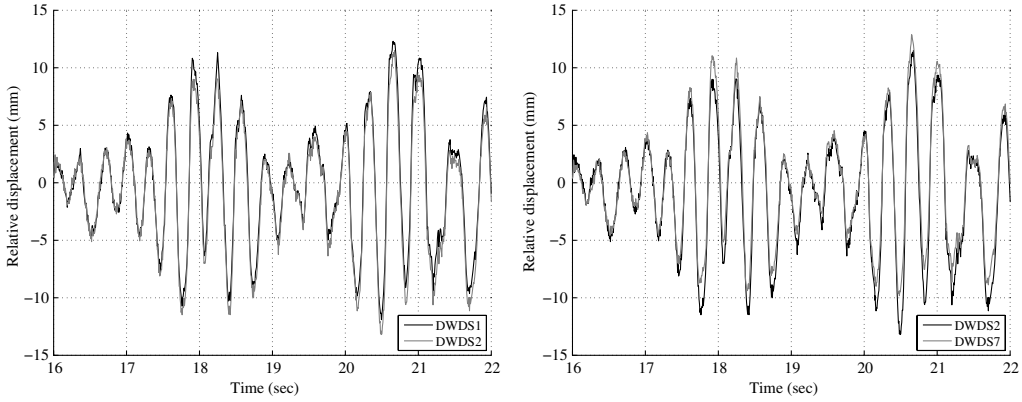

(a) E-W Symmetry (b) N-S Symmetry

Figure 14. Comparison of relative displacements obtained by DWDS.

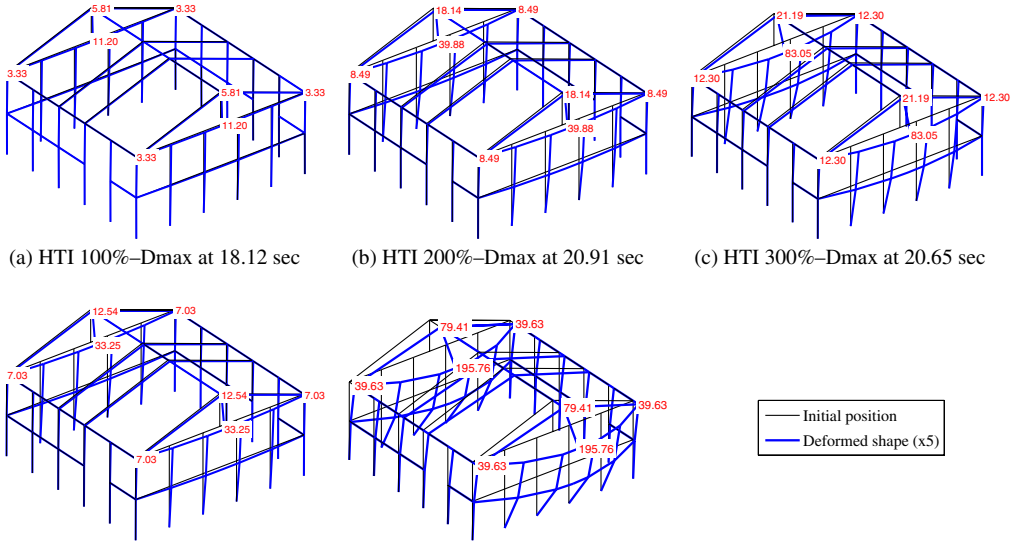

(a) HTI 100%–Dmax at 18.12 sec (b) HTI 200%–Dmax at 20.91 sec (c) HTI 300%–Dmax at 20.65 sec

(d) GUA 100%–Dmax at 23.48 sec (e) GUA 390%–Dmax at 23.55 sec

Figure 15. Global deformations (mm) obtained at the time when the transverse wall displacement is maximized.

between wall and roof are quite flexible (ligature wires and common nails). As a reminder, this structure has been adapted from Haiti's local building culture through the use of short pieces of wood and basic connection techniques. This phenomenon may be substantially mitigated by constructing a floor; this kind of house has already served to build granaries above the living area.

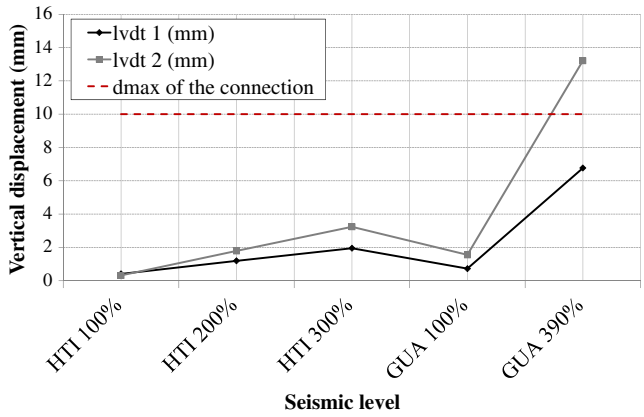

Figure 16. Maximum vertical deformations (mm) experienced by type-1 joints.

- The shear walls are efficient in bracing the structure in the direction of the seismic loading and merely sustained little damage. The type 1 connections reached their tensile strength only during the GUA 390% test (Figure 16), although no damage was visible. The maximum displacement indicated in Figure 16 was obtained from the tension tests presented in Vieux-Champagne et al. (2014).

Global Hysteretic Responses

Figure 18 exhibits the diagram of the base shear versus the top transverse wall displacement. This base shear was computed by summing the inertia forces of the infill on the basis of horizontal acceleration recordings. Since the mass is evenly distributed along the walls, the distribution shown in Figure 17 has been considered herein. For each elementary cell with infill, the weight of the cell (roughly 150 kg) was evenly divided at its four corners (i.e., at the intersection of the wood structure where the accelerometers had been installed). The maximum base shear and displacement obtained are identified by a red circle on each graph.

Figure 18f shows the evolution in the effective lateral stiffness of the transverse wall after each ground motion [called "global hysteresis response" (GHR) in the graph caption], along with a comparison to the normalized lateral stiffness obtained from results of the frequency response function (FRF). The effective stiffness values have been derived by computing the slope connecting the positive and negative peak base shear forces and the corresponding displacement from the graphs in Figure 18. To compare these results, the following assumption was made: The effective stiffness obtained for HTI 100% of GHR and FRF are equal.

The hysteretic responses of the structure recorded during the HTI and GUA series highlight the trend in the case of a nonlinear overall behavior. For HTI 100%, the overall behavior is linear, thus highlighting that the structure is highly resistant to a ground motion equivalent to the January 12 Haiti earthquake. The slight decrease in natural frequency

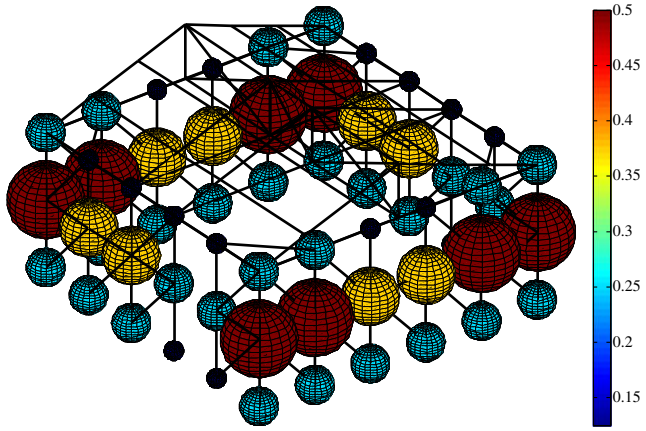

Figure 17. Assumption of the mass distribution to take into account the inertia forces.

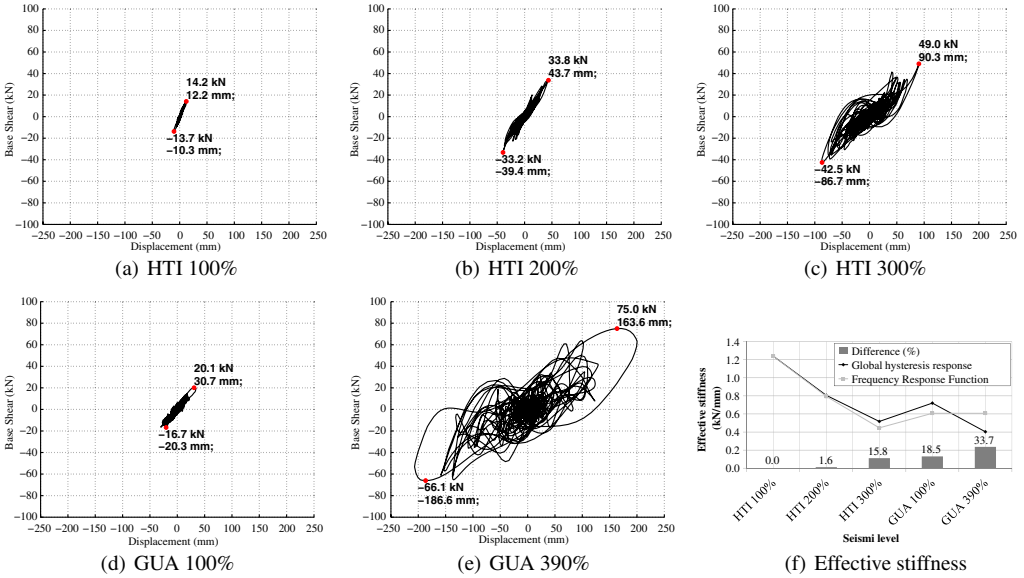

(a) HTI 100% (b) HTI 200% (c) HTI 300%

(d) GUA 100% (e) GUA 390% (f) Effective stiffness

Figure 18. Global hysteretic responses of the transverse wall.

observed in Figure 9 for HTI 100% assimilated with structural rearrangement is no longer visible here. The nonlinearity and dissipated energy increase as stiffness decreases (Figure 18f) after each HTI 200% and HTI 300% signal, which reveals the structural damage (Section 4.3). Following the reparation and during GUA 100%, the overall

behavior did not fully recover its linear behavior, and its effective stiffness has only risen slightly relatively to HTI 300%. This finding can be explained by the irreparable damage sustained by the wood–infill interface and infill degradation, as well as by the local deformation of wood at the metal connectors. The overall behavior observed during GUA 390% reflects a typical hysteresis curve with good seismic resistance (to the considerable seismic ground motion).

From Figure 18f, it can be noted that the effective stiffness obtained with the results of GHR and FRF yield similar results except for GUA 390%, whose GHR seems to provide more plausible results since damage observed during this test was the most significant.

Figure 19 also depicts the diagram of the base shear versus the top shear wall displacement. The same observations as in Figure 18 are applicable here: The connection between the behavior of the shear wall and the transverse wall can again be highlighted. Figure 19f shows the evolution in the effective lateral stiffness of the shear wall and transverse wall after each ground motion and moreover indicates the ratio between the effective stiffness obtained for the shear wall and that for the transverse wall. This figure underscores the similar evolution of both curves with the ratio between each pair of values varying between 4.5 and 7.3. It can also be inferred that the behavior of the shear wall benefits from less damage than the transverse wall; hence, the reparation process exerts less influence on its behavior.

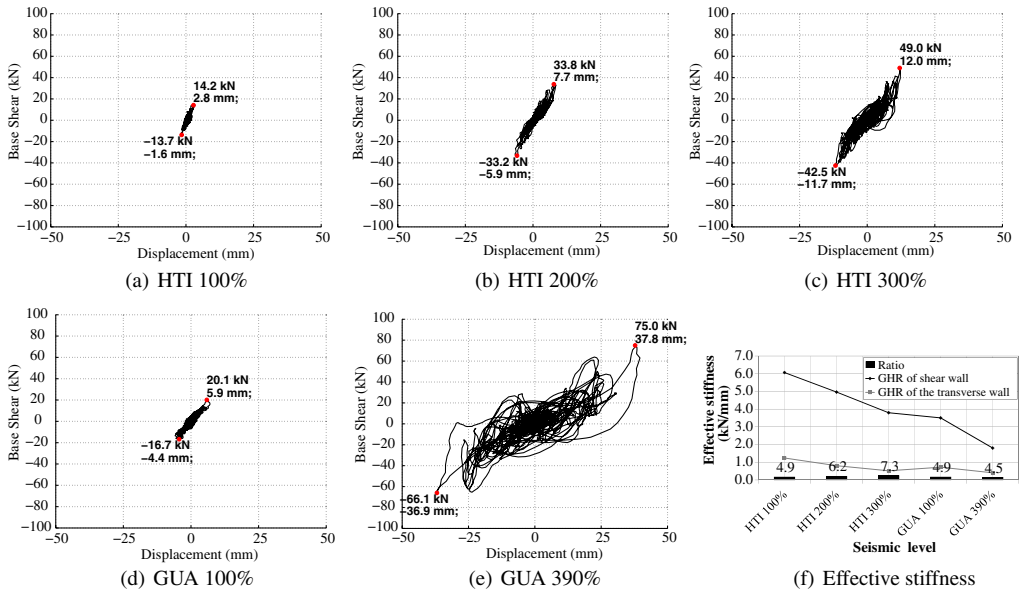

Figure 19. Global hysteretic responses of the shear wall.

OBSERVED DAMAGE

The observed damage is described in Table 3 and Figure 20. During the HTI series, little damage was noticeable, and all of it was due to deformation of the transverse walls and roof structure. The steel strip bent and its nails were extracted by several millimeters. At the top center of the transverse walls, the infill begins to fail and two stones collapse during the HTI 300%. Otherwise, the roof structure remained flexible thanks to the slenderness of the bracings and common nail connections, which could be pulled out relatively easily (not the case during HTI 100%). After the reparation, the structure sustained little damage during GUA 100%, with another pull-out of the roof structure bracing. Lastly, the ground motion GUA 390% heavily damaged the structure with, in particular, a collapse of two infill triangles on a transverse wall. The horizontal bracing between the eastern shear wall and the northern transverse wall was stripped (Figure 20f). The shear wall damage was visible from GUA 390%. Some infill triangles began to pull out from the wood structure (Figure 20k), and damage in the type 1 connection was indeed significant, as shown in Figure 20i and emphasized again in Figure 16.

Table 3. Observed damage

Ground motion	Infill	Type-1 connection	Ligature wire	Roof structure	Horizontal bracing
HTI 100%	—	—	—	—	—
HTI 200%	Top sill–infill separation	Light bending of steel strip and nails extracted (2–3 mm) (Figure 20b)	—	Slight extraction of vertical stud and bracing (Figure 20c)	—
HTI 300%	Collapse of two stones (Figure 20d)—failure of the mortar at the top sill–infill separation	Nails extracted (Figure 20e)	Ligature wires loosened	Pull out of a bracing	Slight ligature deformation and local wood deformation
Reparation operation					
GUA 100%	—	—	—	Pulled out of a bracing	—
Reparation operation					
GUA 390%	Damage and collapse of two triangle cells of infill (Figures 20h and 20k)	Bending of steel strip and nails pull off (Figures 20g and 20i)	Ligature wires loosened and detached (Figure 20j)	Buckling failure of a bracing – Celling joist pulled out (Figure 20l)	Bracing pulled out (Figure 20f)

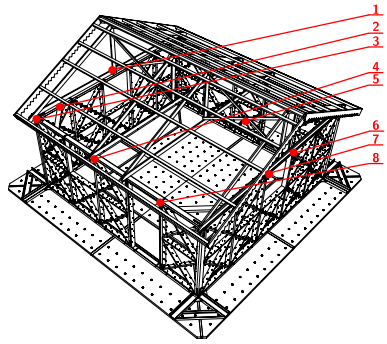

(a) Damage location

(b) HTI 200%: Connection–Location 6: North transv.wall

(c) HTI 200%: Roof bracing–Location 1: South transv.wall

(d) HTI 300%: Filling–Location 7: South transv.wall

(e) HTI 300%: Connection–Location 7: South transv. wall

(f) GUA 390%: Bracing–Location 2: North transv.wall

(g) GUA 390%: Connection–Location 7: South transv.wall

(h) GUA 390%: Filling Location: South transv.wall

(i) GUA 390%: Connection–Location 4: West shear wall

(j) GUA 390%: Ligature wire–Location 8: West shear wall

(k) GUA 390%: Infill–Location 5: East shear wall

(l) GUA 390%: Celling joist –Location 3: Roof

Figure 20. Damage.

CONCLUSION

This paper has presented the last step of a multiscale experimental program (Vieux-Champagne et al. 2014) aimed at testing the entire structure. To the best of the authors' knowledge, this seismic testing campaign is the first one ever performed on a timber-framed structure with infill. For this purpose, the campaign has focused on experimental observations along with an analysis based on free vibration tests and seismic tests.

To conduct this test, a seismic ground motion has been designed by the Nice-based CEREMA (France) to subject the structure to a seismic hazard similar to the one that occurred on 2010 January 12 in Haiti (due to the context of this study). Subsequently, a seismic ground motion representative of high seismic hazard zones found in the Antilles was used.

The free vibration tests allowed detecting the first three natural frequencies of the building and their evolution after each seismic ground motion. From these results, damage was identified; moreover, some characteristic seismic values were computed (e.g., the effective lateral stiffness and the equivalent viscous damping ratio).

The global response of the building was analyzed through the results of displacement measurement sensors (DWDS, LVDT, and DIC) and accelerometers. First, the DIC was validated from DWDS results by virtue of the authors' knowledge: This was the method's first successful implementation at this scale. These databases made it possible to plot a three-dimensional view of the global deformation and to better understand the overall structural behavior. The transverse wall deformation was especially important for its dimensions due to the lack of horizontal bracing in the structure, whose design had been based on existing Haitian structures. On the other hand, the transverse wall did not fail after the five seismic ground motions; however, two infill triangles collapsed, which could have been harmful for dwelling occupants. This issue would not be any more serious for multistory buildings since the floor, rigid in comparison to the transverse wall, would limit the effect and prevent against deformation accumulation. The shear walls underwent only limited deformation (at the top of the walls) and adequately braced the structure. For instance, the maximum displacement was 45 mm for GUA 390%, whereas a modern timber-framed wall [OSB12 panels with 1.5 tons at the top of the wall (Humbert et al. 2014 and Boudaud et al. 2014)] reaches 44 mm for GUA 320% (and in similar experimental configurations: ground motion, shake table, etc.). The global hysteretic response has been analyzed through the base shear versus the top displacement of both the transverse wall and shear wall. These results served to highlight the similar shape of the hysteretic responses of both walls, which experienced significant deformation and dissipated a large amount of energy. The lateral effective stiffness was computed on the basis of hysteretic response results, in demonstrating the evolution of damage after each ground motion. An interesting correlation has been drawn between the results obtained from the GHR and FRF, revealing that FRF can provide significant results as regards the evolution in structural behavior after each ground motion. The seismic vulnerability of the transverse wall was then pointed out by comparing its effective stiffness evolution to that of the shear wall.

The last section focused on damage observed during the experimental campaign. It was revealed that the main damage was located in the steel connectors and infill. After each ground motion, the nailed connections did in fact began to pull out, especially at the top

of the transverse walls and on the roof structure. The damaged infill panels confirm that a substantial amount of energy was dissipated both in the panels and at their interface with the wood structure. In the case of the shear wall, the infill damage was limited. The behavior of infill during seismic ground motion therefore is particularly valuable since it enhances the lightweight wood structure's efficiency in resisting highly harmful ground motion while sustaining only minor overall damage due to fiber reinforcement of the earth. It must be pointed out however that for the ground motion GUA 390% (Figure 20k), two infill panels were pulled-out out-of-plane, which is a key issue in preventing injury to dwelling occupants, even though this risk is technically easy to mitigate (e.g., a wire mesh nailed onto the inner face of the wall).

This article has confirmed that timber-framed structures with infill exhibit relatively high seismic resistance and, thanks to the shake table test, provide direct proof to the scientific community as well as to those leading reconstruction efforts in Haiti and elsewhere that this type of structure, in relying on local knowledge, can be used in new construction. Moreover, this article enhances the state of knowledge of seismic-resistant behavior relative to traditional wood-framed structures with infill.

This experimental campaign at the 4-scale of the structure contributes relevant results to completing not only the analysis performed at scales 1, 2, and 3 (Figure 1) but also the experimental multi-approach that allows developing a model to predict the behavior and assess the vulnerability of timber-framed structures with infill under seismic loading conditions.

ACKNOWLEDGMENTS

The authors wish to thank and acknowledge the support of the French National Research Agency (ANR) for the ReparH project under reference code ANR-10-HAIT-003 (coordinated by CRAterre in collaboration with UJF-3SR, and the AE&CC research Unit of ENSAG and the Haitian NGO GADRU), the participating associations of the PADED platform, and all local partners for their involvement and participation, contributing to this research project. This work is supported by a public grant overseen by the French National Agency as part of the "Investissements d'Avenir" program (reference: ANR-10-LABX-0083). The laboratory 3SR is part of the LabEx Tec 21 (Investissements d'Avenir; reference: ANR-11-LABX-0030). The authors wish to thank and acknowledge Sadrac St Fleur and Franoise Courboulex, who participated to the simulation of the Haitian ground motion. The authors also thank the technical staffs of the FCBA for the tests they conducted. Gratitude is extended to Simon Pla for his valuable assistance during the experimental program.

REFERENCES

Aki, K., 1967. Scaling law of seismic spectrum, *Journal of Geophysical Research* **72**, 1217–1231.

Aktaş, Y. D., Akyüz, U., Türer, A., Erdil, B., and Güçhan, N. Ş, 2013. Seismic resistance evaluation of traditional Ottoman timber-frame Himishouses: Frame loadings and material tests, *Earthquake Spectra* **30**, 1711–1732.

Ali, Q., Schacher, T., Ashraf, M., Alam, B., Naeem, A., Ahmad, N., and Umar, M., 2012. In-plane behavior of full scale Dhajji walls (wooden braced with stone infill) under quasi static loading, *Earthquake Spectra* **28**, 835–858.

Altidor, J., Dieuseul, A., Ellsworth, W., Given, D., Hough, S., Janvier, M., Maharrey, J., Meremonte, M., Mildor, B., Prepetit, C., and Yong, A., 2010. Seismic monitoring and post-seismic investigations following the 12 January 2010 Mw 7.0 Haiti Earthquake, *AGU Fall Meeting Abstracts* **1**, 7.

Audefroy, J. F., 2011. Haiti: Post-earthquake lessons learned from traditional construction, *Environment and Urbanization* **23**, 447–462.

Bahmani, P., van de Lindt, J. W., Gershfeld, M., Mochizuki, G. L., Pryor, S. E., and Rammer, D., 2014. Experimental seismic behavior of a full-scale four-story soft-story wood-frame building with retrofits. I: Building design, retrofit methodology, and numerical validation, *Journal of Structural Engineering* **142**.

Beauval, C., Honoré, L., and Courboulex, F., 2009. Ground-motion variability and implementation of a probabilistic–deterministic hazard method, *Bulletin of the Seismological Society of America* **99**, 2992–3002.

Beeler, N., Wong, T.-F., and Hickman, S., 2003. On the expected relationships among apparent stress, static stress drop, effective shear fracture energy, and efficiency, *Bulletin of the Seismological Society of America* **93**, 1381–1389.

Bertil, D., Rey, J., and Belvaux, M., 2010. *Projet ANR SISBAT – Modélisation de l'Action Sismique, Rapport Final BRGM/RP-58886-FR*.

Boore, D. M., 1983. Stochastic simulation of high-frequency ground motions based on seismological models of the radiated spectra, *Bulletin of the Seismological Society of America* **73**, 1865–1894.

Boudaud, C., Humbert, J., Baroth, J., Hameury, S., and Daudeville, L., 2014. Joints and wood shear walls modelling II: Experimental tests and FE models under seismic loading, *Engineering Structures* **101**, 743–749.

Brune, J. N., 1970. Tectonic stress and the spectra of seismic shear waves from earthquakes, *Journal of Geophysical Research* **75**, 4997–5009.

Ceccotti, A., Faccio, P., Nart, M., and Simeone, P., 2004. Seismic behavior of wood framed buildings in Cadore mountain region—Italy, in *13th World Conference on Earthquake Engineering*, Vancouver, BC, Canada, Paper No. 4011.

Clough, R. W., and Penzien, J., 1993. *Dynamics of Structures*, McGraw-Hill, New York.

Combe, G., and Richefeu, V., 2013. TRACKER: A particle image tracking (PIT) technique dedicated to nonsmooth motions involved in granular packings, in *AIP Conference Proceedings* (A. Yu, K. Dong, R. Yang, S. Luding, Editors) **1542**, 461–464.

Cruz, H., Moura, J. P., and Machado, J. S., 2001. The use of FRP in the strengthening of timber reinforced masonry load-bearing walls, in *Proceedings of Historical Constructions, Guimarães, Portugal*, Academic Press.

Dogangun, A., Tuluk, O., Livaoglu, R., and Acar, R., 2006. Traditional wooden buildings and their damages during earthquakes in Turkey, *Engineering Failure Analysis* **13**, 981–996.

Dutu, A., Gomes Ferreira, J., Guerreiro, L., Branco, F., and Goncalves, A., 2012. Timbered masonry for earthquake resistance in Europe, *Materiales de Construccion* **62**, 615–628.

EN 10230-1, 2000. *Steel Wire Nails—Part 1: Loose Nails For General Applications.*

EN 1998-1, 2005. *Design of Structures for Earthquake resistance—General Rules, Seismic Actions and Rules for Buildings.*

EN 338, 2003. *Structural Timber—Strength Classes*.

Ferreira, J., Teixeira, M., Du u, A., Branco, F., and Gonçalves, A., 2012. Experimental evaluation and numerical modelling of timber-framed walls, *Experimental Techniques* **38**, 45–53.

Filiatrault, A., Christovasilis, I. P., Wanitkorkul, A., and van de Lindt, J. W., 2009. Experimental seismic response of a full-scale light-frame wood building, *Journal of Structural Engineering* **136**, 246–254.

Filiatrault, A., Fischer, D., Folz, B., and Uang, C.-M., 2002. Seismic testing of two-story woodframe house: Influence of wall finish materials, *Journal of Structural Engineering* **128**, 1337–1345.

Gurpinar, A., Erdik, M., and Ergunay, O., 1981. Siting and structural aspects of adobe buildings in seismic areas, IN *Proceedings, International Workshop, Earthen Buildings in Seismic Areas*, 24–28 May, 1981, Albuquerque, New Mexico.

Hartzell, S. H., 1978. Earthquake aftershocks as Green's functions, *Geophysical Research Letters* **5**, 1–4.

Hough, S. E., Altidor, J. R., Anglade, D., Given, D., Janvier, M. G., Maharrey, J. Z., Meremonte, M., Mildor, B. S.-L., Prepetit, C., and Yong, A., 2010. Localized damage caused by topographic amplification during the 2010 M7.0 Haiti earthquake, *Nature Geoscience* **3**, 778–782.

Humbert, J., Boudaud, C., Baroth, J., Hameury, S., and Daudeville, L., 2014. Joints and wood shear walls modelling I: Constitutive law, experimental tests and FE model under quasi-static loading, *Engineering Structures* **65**, 52–61.

Kanamori, H., and Rivera, L., 2004. Static and dynamic scaling relations for earthquakes and their implications for rupture speed and stress drop, *Bulletin of the Seismological Society of America* **94**, 314–319.

Kohrs-Sansorny, C., Courboulex, F., Bour, M., and Deschamps, A., 2005. A two-stage method for ground-motion simulation using stochastic summation of small earthquakes, *Bulletin of the Seismological Society of America* **95**, 1387–1400.

Lambert, M., Gaudin, J., and Cohen, R., 1987. Carte Geologique D'Haiti, Feuille Sud-Est: Port-au-Prince, 1: 250,000, CERCG IMAGEO, CNRS, Paris (Digital image and georeferencing: John Walker, Matraco-Colorado Holding Ltd, 2003).

Langenbach, R., 2006. Preventing pancake collapses: Lessons from earthquake-resistant traditional construction for modern buildings of reinforced concrete, in *International Disaster Reduction Conference (IRDC)*, Davos, Switzerland.

Langenbach, R., 2007. From opus craticiumto the Chicago frame: Earthquake-resistant traditional construction, *International Journal of Architectural Heritage* **1**, 29–59.

Langenbach, R., 2008. Learning from the past to protect the future: Armature crosswalls, *Engineering Structures* **30**, 2096–2100.

Makarios, T., and Demosthenous, M., 2006. Seismic response of traditional buildings of Lefkas Island, Greece, *Engineering Structures* **28**, 264–278.

Meireles, H., Bento, R., Cattari, S., and Lagomarsino, S., 2012. A hysteretic model for frontal walls in Pombalino buildings, *Bulletin of Earthquake Engineering* **10**, 1481–1502.

Ordaz, M., Arboleda, J., and Singh, S. K., 1995. A scheme of random summation of an empirical Green's function to estimate ground motions from future large earthquakes, *Bulletin of the Seismological Society of America* **85**, 1635–1647.

Paultre, P., Calais, É., Proulx, J., Prépetit, C., and Ambroise, S., **2013**. Damage to engineered structures during the 12 January 2010, Haiti (Léogâne) earthquake 1, *Canadian Journal of Civil Engineering* **40**, 1–14.

Poletti, E., and Vasconcelos, G., 2014. Seismic behaviour of traditional timber frame walls: Experimental results on unreinforced walls, *Bulletin of Earthquake Engineering* **13**, 885–916.

Qu, Z., Dutu, A., Zhong, J., and Sun, J., 2014. Seismic damage of masonry infilled timber houses in the 2013 M7. 0 Lushan earthquake in China, *Earthquake Spectra* **31**, 1859–1874.

Sieffert, Y., Vieux-Champagne, F., Grange, S., Garnier, P., Duccini, J.-C., and Daudeville, L., 2016. *Traditional Timber-Framed Infill Structure Experimentation with Four Scales Analysis (To Connection from a House Scale)*, Springer International Publishing, Cham, Switzerland, 287–297.

Tobriner, S., 2000. Wooden architecture and earthquakes in Turkey: A reconnaissance report and commentary on the performance of wooden structures in the Turkish earthquakes of 17 August and 12 November 1999, *International Conference on the Seismic Performance of Traditional Buildings, Istanbul, Turkey*, 16–18.

Van de Lindt, J. W., Bahmani, P., Mochizuki, G., Pryor, S. E., Gershfeld, M., Tian, J., Symans, M. D., and Rammer, D., 2014. Experimental seismic behavior of a full-scale four-story soft-story wood-frame building with retrofits. II: Shake table test results, *Journal of Structural Engineering* **142**.

Van de Lindt, J. W., Pei, S., Pryor, S. E., Shimizu, H., and Isoda, H., 2010. Experimental seismic response of a full-scale six-story light-frame wood building, *Journal of Structural Engineering* **136**, 1262–1272.

Vasconcelos, G., Poletti, E., Salavessa, E., Jesus, A. M., Loureno, P. B., and Pilaon, P., 2013. In-plane shear behaviour of traditional timber walls, *Engineering Structures* **56**, 1028–1048.

Vieux-Champagne, F., Sieffert, Y., Grange, S., Polastri, A., Ceccotti, A., and Daudeville, L., 2014. Experimental analysis of seismic resistance of timber-framed structures with stones and earth infill, *Engineering Structures* **69**, 102–115.

Wennerberg, L., 1990. Stochastic summation of empirical Green's functions, *Bulletin of the Seismological Society of America* **80**, 1418–1432.

Youngs, R., Chiou, S.-J., Silva, W., and Humphrey, J., 1997. Strong ground motion attenuation relationships for subduction zone earthquakes, *Seismological Research Letters* **68**, 58–73.

(Received 5 January 2016; accepted 22 December 2016)